HDL-TM-82-6

August 1982

Stress Analysis of the M735 Proximity Fuze

by Steven A. Boring
John M. Miller

U.S. Army Electronics Research
and Development Command
Harry Diamond Laboratories
Adelphi, MD 20783

The findings in this report are not to be construed as an official Department of the Army position unless so designated by other authorized documents.

Citation of manufacturers' or trade names does not constitute an official indorsement or approval of the use thereof.

Destroy this report when it is no longer needed. Do not return it to the originator.

UNCLASSIFIED

SECURITY CLASSIFICATION OF THIS PAGE *(When Data Entered)*

REPORT DOCUMENTATION PAGE		READ INSTRUCTIONS BEFORE COMPLETING FORM
1. REPORT NUMBER HDL-TM-82-6	2. GOVT ACCESSION NO.	3. RECIPIENT'S CATALOG NUMBER
4. TITLE *(and Subtitle)* Stress Analysis of the M735 Proximity Fuze		5. TYPE OF REPORT & PERIOD COVERED 6. PERFORMING ORG. REPORT NUMBER
7. AUTHOR(s) Steven A. Boring John M. Miller		8. CONTRACT OR GRANT NUMBER(s)
9. PERFORMING ORGANIZATION NAME AND ADDRESS Harry Diamond Laboratories 2800 Powder Mill Road Adelphi, MD 20783		10. PROGRAM ELEMENT, PROJECT, TASK AREA & WORK UNIT NUMBERS Program Ele: 6.46.03A
11. CONTROLLING OFFICE NAME AND ADDRESS U.S. Army Armament R&D Command Picatinny Arsenal Dover, NJ 07801		12. REPORT DATE August 1982 13. NUMBER OF PAGES 30
14. MONITORING AGENCY NAME & ADDRESS*(if different from Controlling Office)*		15. SECURITY CLASS. *(of this report)* UNCLASSIFIED 15a. DECLASSIFICATION/DOWNGRADING SCHEDULE

16. DISTRIBUTION STATEMENT *(of this Report)*

Approved for public release; distribution unlimited.

17. DISTRIBUTION STATEMENT *(of the abstract entered in Block 20, if different from Report)*

18. SUPPLEMENTARY NOTES

DRCMS Code: 6646036630012
DA Proj: 1X464603D663
PRON: 161282286011AA9
HDL Proj: 639162

19. KEY WORDS *(Continue on reverse side if necessary and identify by block number)*

M735 proximity fuze	NASTRAN
Artillery	Finite element
Stress	Structure

20. ABSTRACT *(Continue on reverse side if necessary and identify by block number)*

Structural analysis of the M735 fuze was performed for the gun-firing interior ballistics environment. Because of the complexity of many of the fuze parts, the NASTRAN finite-element computer program was used extensively. Maximum stress and deflection levels were computed and resulting structural safety factors were determined. Several highly stressed parts were instrumented with strain gages and statically tested for correlation with the analytical predictions. The analyses and tests indicated that a structurally efficient fuze design has been achieved.

DD FORM 1 JAN 73 1473 EDITION OF 1 NOV 65 IS OBSOLETE

UNCLASSIFIED

SECURITY CLASSIFICATION OF THIS PAGE *(When Data Entered)*

CONTENTS

FIGURES

FIGURES (Cont'd)

Page

TABLES

1. INTRODUCTION

The M735 fuze, shown in figure 1, is a state-of-the-art electronic proximity fuze now in production for the M753 8-in. nuclear artillery projectile. Extensive structural analyses and tests were conducted during the development program because of the high safety and reliability requirements, complexity of the fuze design, severe gunfiring environmental requirements, and tight weight and volume constraints. The structural analysis and test program was an integral part of the structural design process as described below.

The first step in the structural design of the fuze was the stress analysis of the major structural parts, based on design layouts and drawings. Because of the complexity and constraints mentioned above, an accurate computerized stress analysis was required. Most of the structural parts of the fuze were analyzed with the National Aeronautics and Space Administration Structural Analysis (NASTRAN)[1] computer code. Successive analysis iterations used highly detailed finite-element models in order to accurately predict stress and deflection levels in the various structural parts. Based on the analytical results, structural part drawings were refined and subsequently used for the fabrication of prototype hardware. The prototype hardware was then subjected to a series of laboratory stress-strain tests to verify the accuracy of the analytical predictions. Each part was instrumented with strain gages and subjected to various static loads to verify structural adequacy and the analytical results. Subsequently, gunfiring tests were conducted of prototype structural parts and, ultimately, of complete functional fuzes. A previous report[2] describes in detail the structural firing test program.

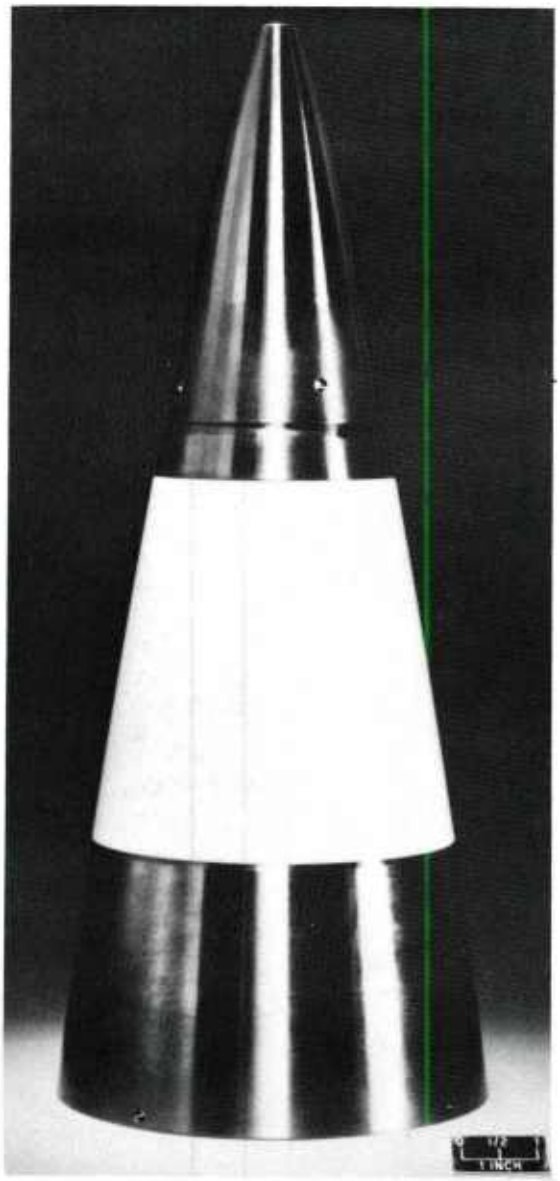

Figure 1. M735 fuze.

This report presents a description and results of the M735 fuze structural analysis. While the structural design and analysis of the fuze was an iterative process, only the analysis of the final design configuration is presented. The mechanical design of the fuze is discussed briefly, preceding a discussion of the structural design requirements and environments, in-

[1] *C. W. McCormick, ed., The NASTRAN User's Manual, National Aeronautics and Space Administration, NASA Sp-222 (October 1969).*

[2] *John M. Miller and Steven A. Boring, Structural Firing Tests of the M735 Proximity Fuze, Harry Diamond Laboratories, HDL-TM-79-6 (May 1979).*

cluding the rationale for assumptions made regarding the environments and their characterization. The analysis of each part or subassembly is discussed in detail, including a description of the analytical model and technique, loading assumptions, boundary conditions, and results. Finally, the static stress testing of the major structural parts is described and those results are compared with the analytical results.

2. M735 FUZE MECHANICAL DESIGN

The M735 fuze must reliably provide programmed power for all projectile components, accurate height sensing for warhead initiation, and in-flight safety. These requirements are met by a dual-channel fuze system, including target sensor, electronic programmer, and power supply assemblies. The electronic assemblies and components are packaged within the fuze, as shown in figures 2 and 3. The fuze consists of three major assemblies: (1) the nose section, which contains the programmer memory/timing (M/T) printed wiring boards (PWBs) and power supplies (fig. 4), (2) the center assembly, which contains the target sensor and E1 assemblies (fig. 5), and (3) the rear assembly, which contains the programmer power-output and decode PWBs (fig. 6).

Figure 2. M735 fuze, partially disassembled.

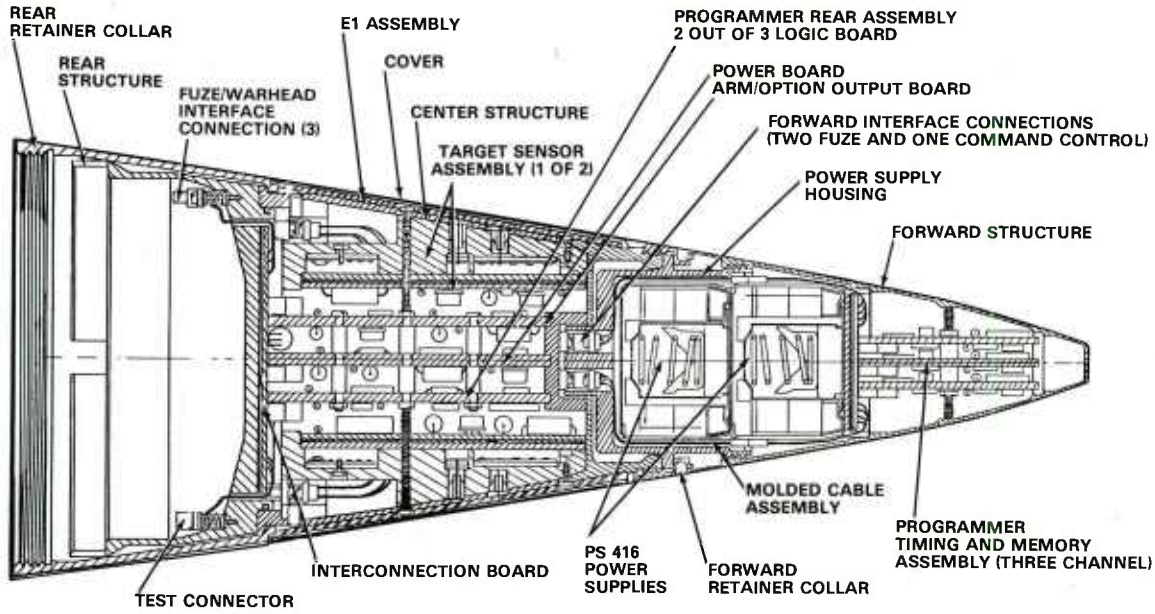

Figure 3. M735 fuze, cross-section view.

The primary structural parts of the fuze are as follows:

(a) the forward structure, which clamps the power supplies and M/T assembly to the power supply housing and provides the proper external ballistic profile,

(b) the power supply housing, which supports the PS416 power supplies, M/T assembly, and forward structure,

(c) the forward retainer collar, which fastens the entire nose section to the fuze projectile section,

(d) the center structure, which supports the entire nose section, target sensors, and E1 assembly, which is bonded to its outer surface,

(e) the rear structure, which supports the programmer power-output and decode PWBs, center assembly, and nose section, and

(f) the retainer collar, which fastens the entire fuze to the projectile.

In addition, all the PWBs of the fuze are structural members, supporting their own inertia and that of the electronic components. In this regard, the M735 fuze is atypical of electronic artillery fuzes. Solid potting is not used for support of electronic components and PWBs; instead, a thin layer of polyurethane coating (0.015 in. thick*) is applied to the components for support. The PWBs are designed to be self-supporting, employing numerous brackets, mounting fixtures, fasteners, and greater than normal board thickness (up to 0.125 in.).

*(in.) 25.4 = (mm).

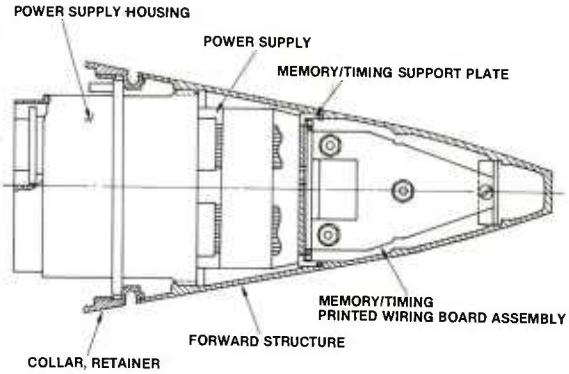

Figure 4. Nose section assembly.

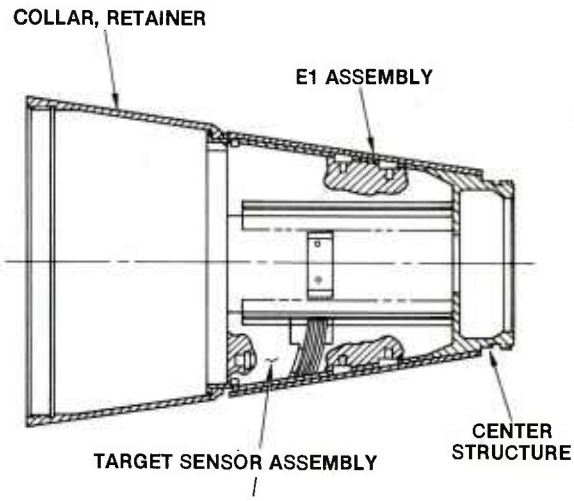

Figure 5. Center assembly.

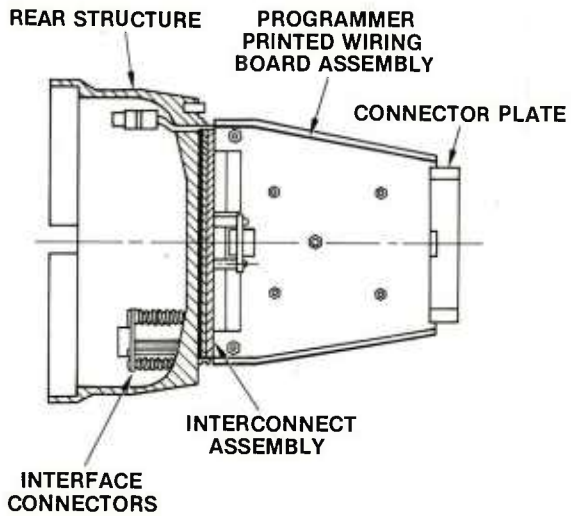

Figure 6. Rear assembly.

3. STRUCTURAL DESIGN REQUIREMENTS

The fuze structure is required to protect the electronic subassemblies and components from degradation and failure due to exposure to the environments specified in the XM753 Projectile Stockpile-to-Target-Sequence (STS).[3] These environments include storage, transportation and handling, gunfiring, and flight. Obviously, the most severe environment is gunfiring, which includes large inertia loadings due to projectile in-bore accelerations. In contrast, the handling and transportation environments consist of relatively low-level accelerations resulting from aircraft and vehicular vibration as well as minor impacts and drops of the projectile in its container. The analysis described in this report is confined to the gunfiring interior ballistic environment.

The 8-in. gunfiring environment consists of the following projectile accelerations:

(a) Setback (10,400 g max)—the axial acceleration of the projectile in the gun. A

[3] *Stockpile-to-Target-Sequence (STS) for the 8-Inch Howitzer/Gun, Nuclear Projectile (XM753), U.S. Army Nuclear and Chemical Agency (April 1978).*

typical acceleration time trace is shown in figure 7.

(b) Angular (164,000 rad/s^2 max)—the angular acceleration imparted to the projectile by the gun-tube rifling. This acceleration is generally proportional to setback. A typical trace is shown in figure 7.

(c) Centripetal acceleration due to the projectile spin rate (195 rps max). Spin reaches the maximum at muzzle exit.

(d) Balloting (1000 g max)—the lateral acceleration of the projectile due to clearance between the projectile bourrelet and the gun-tube rifling. This clearance may result in multiple "slaps" of the projectile against the rifling as it travels up the tube. Balloting is not well understood, and the 1000-g maximum is an assumption based on previous computations performed by the U.S. Army Armament R&D Command (ARRADCOM).[4]

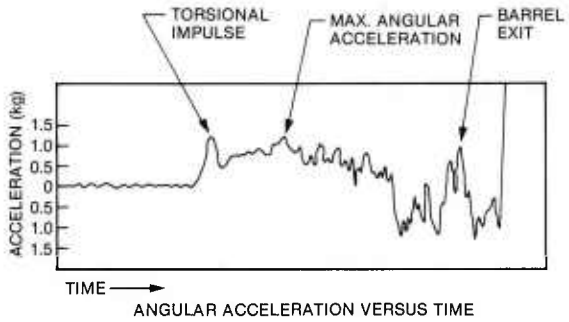

ANGULAR ACCELERATION VERSUS TIME

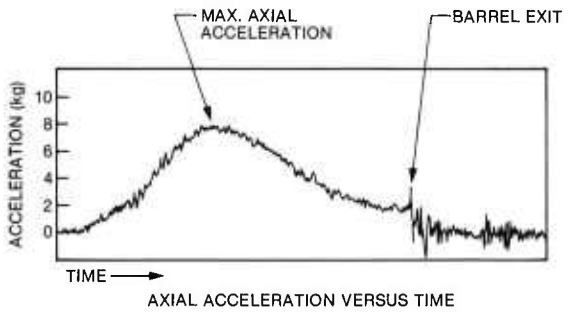

AXIAL ACCELERATION VERSUS TIME

Figure 7. Typical acceleration curves.

(e) Compression-release (2000 g max)—the rebound effect due to the sudden decrease in axial acceleration as the projectile clears the tube muzzle (also referred to as set forward).

(f) Torsional impulse—a short-duration spike of angular acceleration which may occur at the onset of rifling if the projectile is not fully seated when rammed. It was assumed in this analysis that the peak level is less than the maximum angular acceleration which occurs later in the projectile travel up the gun tube.

The inertia loadings resulting from these in-bore accelerations can combine due to the simultaneity of the accelerations. When this is the case, and when a particular structure is susceptible to the combination, this was included in the analysis. For example, the combined effects of spin and balloting (both lateral loads) were examined in the analysis of the vertically mounted PWBs. On the other hand, several structures were analyzed for axial loadings only, since the effects of lateral and angular accelerations were judged to be insignificant. The assumptions made in each case are discussed in the detailed analysis (sect. 5).

4. ANALYTICAL APPROACH

The approach taken here was to initially perform a broad analysis of the overall fuze, including all major structural parts. The purpose of this analysis was (1) to determine whether gross deflections were within allowable limits and (2) to pinpoint highly stressed areas requir-

[4] *Szu Hsuing Chu, Transverse Motion of 8-Inch Projectile XM753 in Gun Tube XM201, Picatinny Arsenal, TR4918 (December 1975).*

ing more detailed analyses. The next step was the detailed analysis of those areas shown to be highly stressed. In addition, those parts which may not be highly stressed but are vulnerable to large deflections were analyzed in detail. This was particularly true of the vertically mounted PWBs. Excessive (greater than 0.02 in.) out-of-plane deflections and deflection gradients of these PWBs can result in the fracturing of electronic components, solder joints, and PWB tracks.

5. DETAILED ANALYSES

5.1 *Overall Fuze*

The overall fuze was analyzed with the NASTRAN finite-element computer code. The major structural parts, including forward structure, power supply housing, center structure, and rear structure, were modeled with conical shell elements, which are symmetrical with respect to the centerline. The electronic assemblies were characterized as nonstructural masses acting on the structural parts at appropriate locations. The model is depicted in figure 8.

The loading condition investigated was limited to the peak axial setback acceleration. The boundary condition of fixed axial motion was applied at the aft end of the rear structure (node 38, fig. 8). The setback loading condition was simulated by applying a 10,400-g "gravity" force in the axial direction.

The key deflection results are shown in figure 8. The maximum deflection of the rear structure (node 34) is 0.044 in. This is well below the maximum allowable 0.060 in. to insure noninterference with mating projectile parts. Other deflections shown are small enough to insure survivabiity. Peak stresses for the various parts and their locations are also shown. The forward structure was found to be very lightly stressed (6 ksi*), indicating that further, more detailed analysis is unnecessary. The other major parts—power supply housing, center structure, and rear structure—all exhibit large stress gradients and relatively high peak stresses: 88, 89, and 74 ksi, respectively. A more thorough and detailed analysis of these parts is necessary. In addition, several other components were not

*(ksi) 6.894 × 10^3 = (kPa).

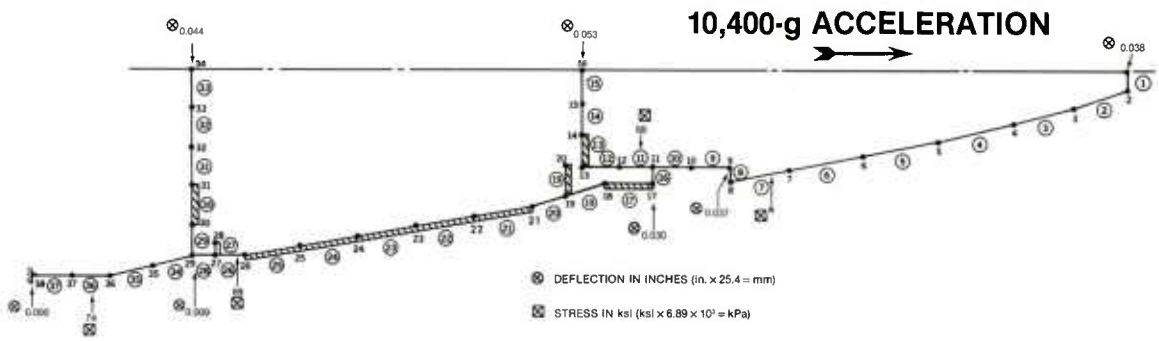

Figure 8. Finite-element model of fuze.

modeled in this analysis, including the M/T PWBs and support plate, programmer PWBs, E1 cover, and collars. These will be investigated in more detail.

5.2 *Nose-Section Assembly*

5.2.1 *Memory/Timing Assembly*

The M/T assembly consists of three epoxy-fiberglass PWB assemblies mounted vertically on an interconnection PWB. The assembly is supported by the titanium alloy (Ti-6Al-6V-2Sn) support plate, which in turn is supported by the top battery in the fuze nose section. The three vertical PWBs are attached to one another at four locations: the board bottom corners with threaded studs and aluminum mounting blocks, near the board center with a threaded stud and with epoxy-fiberglass spacers, and at the top of the board with a bolt-mounted epoxy-fiberglass support. This assembly is attached to the support plate by four screws which are assembled through the support plate from the bottom and threaded into the bottom of the mounting blocks. The mounting blocks are designed to allow a gap between the blocks and the interconnection PWB, thus insuring that the three vertical PWBs are seated on the interconnection PWB. The assembly is restrained in the lateral direction by closely controlled clearances between the forward structure and the center stud, the top support, and the support plate. Forward axial motion is restricted by the forward structure, which clamps the upper rim of the support plate when it is attached to the power supply housing.

The stress analysis of the M/T assembly components involved the analysis of the vertical PWBs for setback, spin, and balloting and the analysis of the support plate for setback and compression-release. The NASTRAN computer code was used for these analyses of each component.

The PWBs are subjected to self-loading generated by the inertia of the PWBs and their electronic components during spin, balloting, and axial acceleration, and are constrained from lateral motion during balloting and spin at the mounting hardware locations. Because of the relatively large axial deflections of the support plate at its center, it can provide support for the M/T PWBs only near its outer edge. Therefore, the setback loads of the boards are transmitted to the support plate at localized points near the bottom corners. The plate is simply supported at the outer diameter by the top battery during setback and by the forward structure during compression-release. During compression-release, the plate carries the weight of the two power supplies at its outer diameter.

The PWBs were modeled with plate elements for the balloting and spin analyses. The plate element has both inplane and bending stiffness for a cross section of a solid homogeneous material. This element has five degrees of freedom (rotation about the axis normal to the surface is not included). Due to symmetry only one-half of each board was modeled, with their centerlines being a boundary condition constrained from motion in the transverse direction as well as from rotation. Figure 9 shows the free-body diagrams and finite-element models.

Axial acceleration produces only inplane stresses and deflections in the vertical PWBs. For this reason they were modeled using membrane elements, which have finite inplane stiffness and zero bending stiffness, for the setback analysis. This results in a more efficient model, requiring less computer computation time than the plate element model. The membrane element is otherwise used in much the same way as the plate element; the only difference in modeling the PWBs for the setback acceleration was to generate a finer mesh at the base of the boards, where higher stresses and stress gradients were expected.

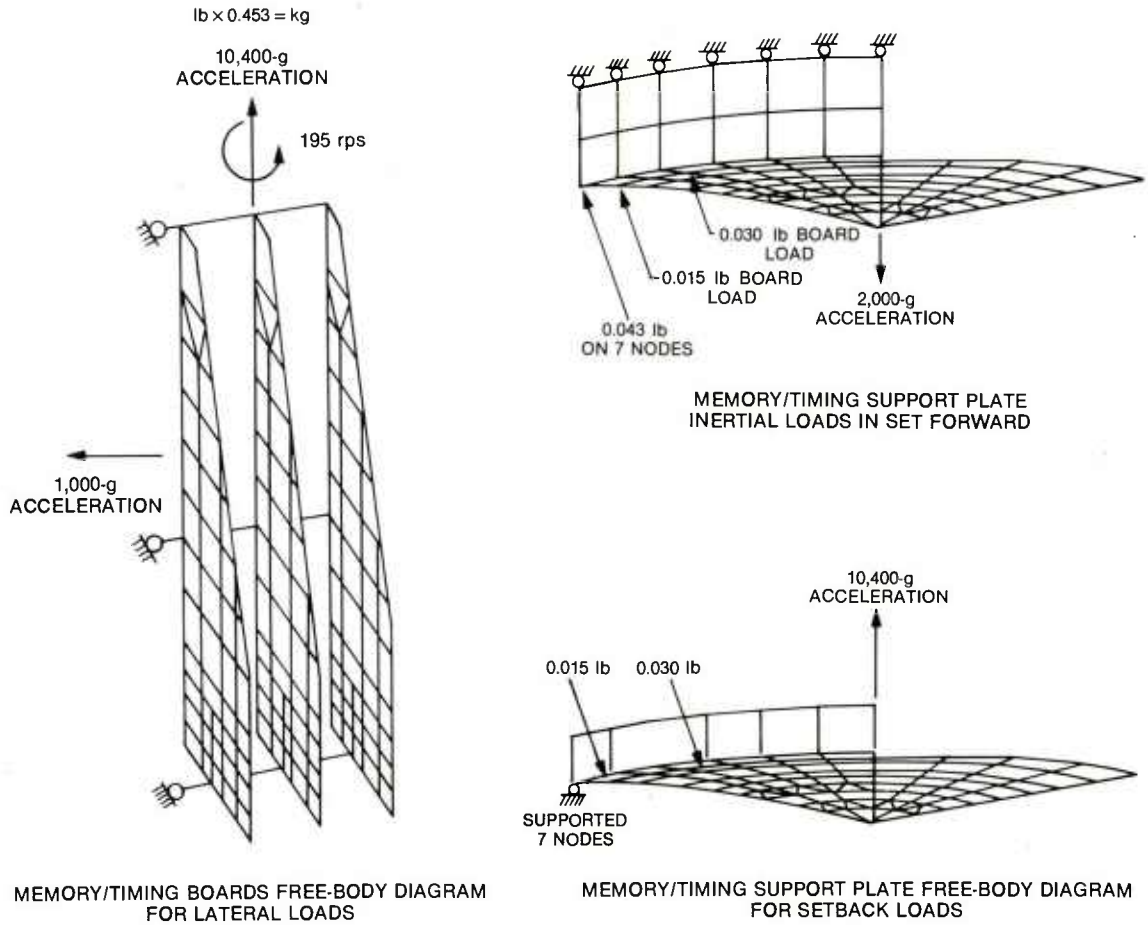

Figure 9. M/T assembly free-body diagrams.

The support plate was modeled with plate elements. Due to the symmetry of this part only one-quarter of the plate was modeled. The cut edge boundaries were constrained from rotation and from translation in the angular direction in addition to the overall constraint of rotation about the axis normal to the surface.

The peak stress in the vertical PWBs occurs during setback and is a compressive stress of 32 ksi at the bottom corners where they are supported. This results in a factor of safety of only 1.09 over the edgewise compressive strength of G-10 epoxy-fiberglass boards. However, the stress quickly decreases to less than 10 ksi just above the mounting block stud hole. This is a very localized high stress in an area where there is no circuitry or components, and therefore is not considered a problem. In comparison, the combined spin and balloting inertial forces produced a maximum stress of only 5.4 ksi near the center support of the outermost PWB. Maximum deflection out of plane was well below the 0.020 allowance.

The analysis of the support plate indicated that the maximum bending stresses occur in the area where the PWBs load the plate in setback. Results of the setback analysis are shown in figure 10. The 135-ksi peak stress is pessimistic, since the top battery supports a larger area of the plate than was assumed in the analysis. Therefore, the minimum factor of safety should actually exceed the 1.20 prediction based on the yield strength of the titanium support plate. Compression-release acceleration results in a maximum compressive stress of 20 ksi in the same area in which the maximum setback stress occurs.

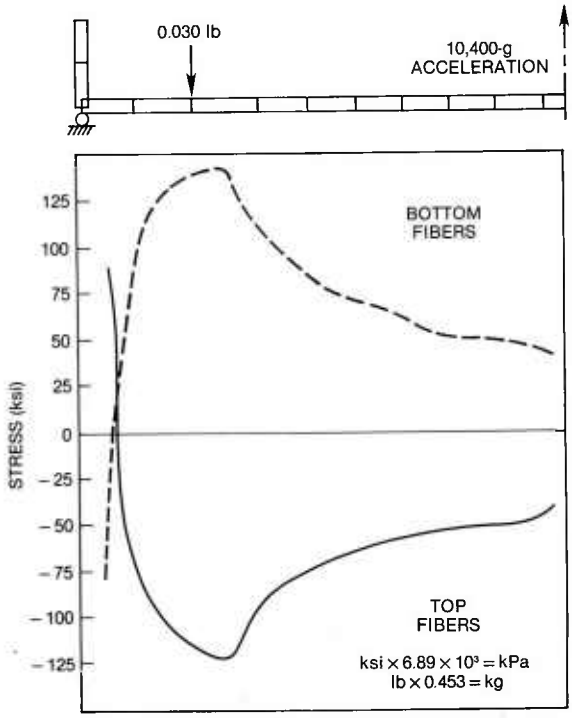

Figure 10. Maximum principal stresses in M/T support plate.

5.2.2 *Power Supply Housing*

The power supply housing is a 6-6-2 titanium machined part which provides structural support for the entire nose-section assembly. The two power supplies are stacked axially within the housing with the M/T assembly supported by the top battery. A flange around the exterior of the housing supports the total weight of the nose assembly on the center structure. The forward structure attaches to threads on the top of the housing. On the base of the housing is a shroud which protects the two interface connectors and also acts as a stiffening member.

The power supply housing was analyzed for setback only, since the other loading conditions do not produce significant stress levels in the housing. The two power supplies and the M/T assembly load the base of the housing near its internal diameter. The forward structure loads the forward threaded end of the housing. These loads, in addition to the self-loading of the housing are transmitted to the center structure at the power supply housing flange.

The housing was analyzed with NASTRAN with plate elements for the side wall, flange, and base and with bar elements for the protective shroud. The bar element permits extension, torsion, and bending in two perpendicular planes and the associated shears. The shear center coincides with the elastic axis of the element. The entire housing was modeled because of the nonsymmetry of the shroud. The finite-element model of the housing is shown in figure 11.

The free-body diagram and plots of the resulting axial and hoop stresses for the housing sidewall are shown in figure 12. The area of highest stress is in the sidewall just below the flange, where axial stress levels of 140-ksi tension and 70-ksi compression occur on the inner and outer surfaces, respectively. The stresses in the shroud range from 81 ksi in the center to 131 ksi at the ends, as shown in figure 13. The maximum bending stress in the base is 85 ksi. The power supply housing provides a factor of safety of 1.15 over yield strength and 1.25 over ultimate strength during setback acceleration.

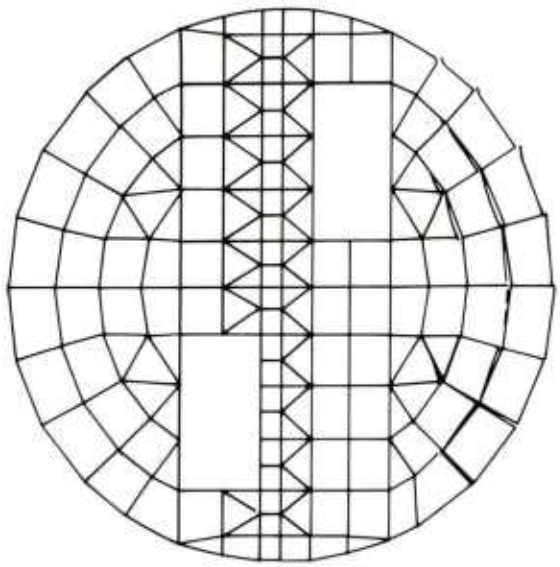

(a) HOUSING BASE ONLY
(SHROUD NOT SHOWN)

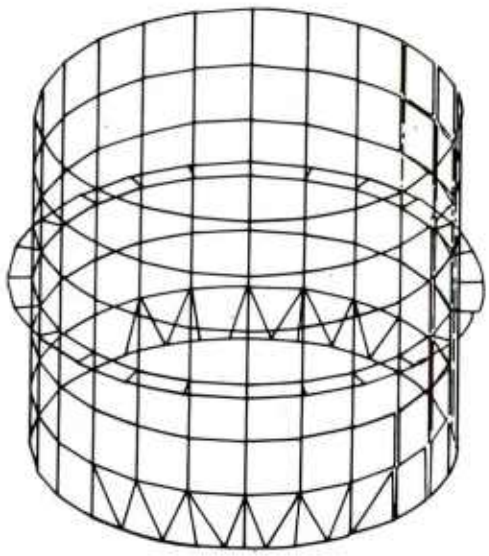

(b) BASE NOT SHOWN

Figure 11. Power supply housing model.

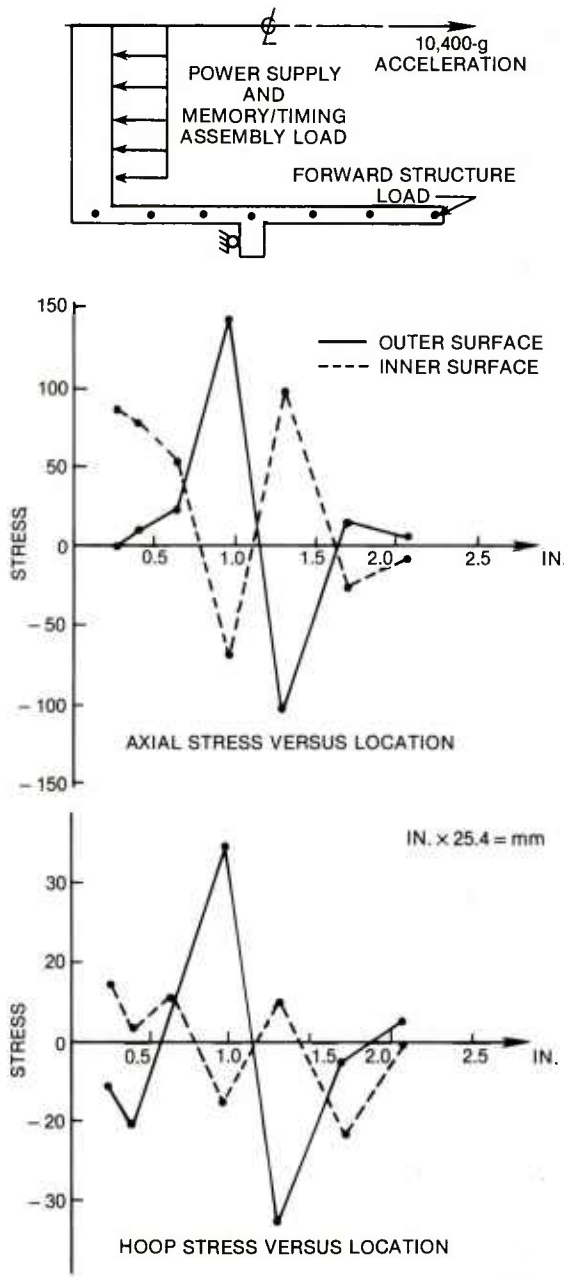

Figure 12. Power supply housing stresses during setback.

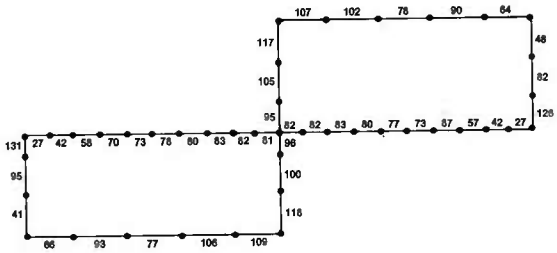

Figure 13. Power supply housing shroud maximum principal stresses.

5.2.3 *Forward Collar*

The forward collar is a 6-6-2 titanium machined part which fastens the nose section to the fuze projectile section. The collar is captured between the power supply housing flange and the rear edge of the forward structure, where a small gap allows free rotational movement. When assembled to the projectile section, the forward collar clamps the power supply housing flange to the forward seating surface of the center surface.

The only loading condition which results in significant stress levels in the forward collar is compression-release, in which the nose-section inertia load is transmitted through the collar. This results in a maximum shear stress of approximately 13 ksi, well within the allowable stress for the material.

5.3 *Center Assembly*

5.3.1 *Center Structure*

The center structure is a 6-6-2 titanium machined part which provides structural support for the nose section and two target sensors. The nose-section power supply housing flange is clamped to the forward seating surface of the center structure by the nose retainer collar. All nose-section axial gun-launch loads are transmitted at this surface. An internal pilot diameter at this same location provides lateral support for the nose. A plate that supports the nose-section mating connectors is mounted to the forward flange of the center structure.

The center structure also provides axial support for the two target sensors which mount on an internal shelf near the aft end. The sensors, with an outside contour which conforms to the inner conical surface of the center structure, are attached to the wall 180 deg apart with two screws each. The clearance holes for the screws in the center structure are elongated in the axial direction to allow for the differential axial deflections of the target sensors and center structure. In addition, the center structure provides structural support for the E1 assembly, which is wrapped around and bonded to the external surface.

The loading conditions which result in significant stress levels in the center structure are setback, balloting, and spin. The center structure was modeled two ways for the NASTRAN analyses of these conditions. The symmetry of the axial setback load enabled the use of the timesaving conical shell elements. The properties of the conical shell element are symmetrical with respect to the axis of the shell. To use this element, a conservative loading assumption was made for the rectangular connector plate cutout on the forward flange. It was modeled as a circular hole with a concentric load representing that portion of the flange not included in the model, plus the connector plate. The axial loads of the nose assembly on the forward seating surface and the target sensors' nonuniform load on the bottom shelf were both assumed to be uniform around their seating surface for this model. For the unsymmetrical loading (balloting and spin), one-half of the structure was modeled with plate elements. The finite-element model is shown in figure 14. In addition, the balloting and spin analyses were performed separately, to analyze the "worst-case" condition for each. The applied loads for balloting included (1) a moment at the forward end due to the inertia of the nose section; (2) the target sensor

loads (a uniform pressure on the interior surface for one sensor and two point loads at the mounting screw locations for the other); and (3) self-loading of the structure and E1 nonstructural mass. Spin loads included the interior pressure due to the target sensors, plus the self-loading of the structure.

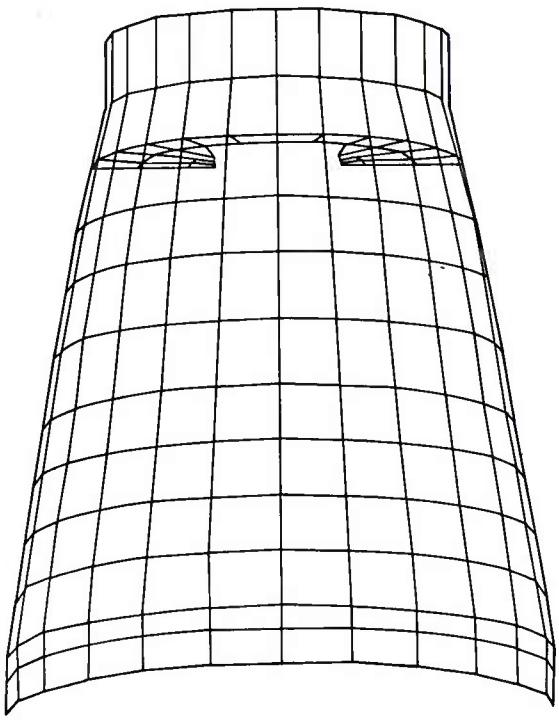

Figure 14. Center structure model.

The free-body diagrams and the analysis results for the center structure loading conditions of setback, spin, and balloting are shown in figures 15, 16, and 17, respectively. The maximum stress (80-ksi compression) occurs during setback near the aft end of the center structure. A combination of balloting and setback could produce a stress level of 110-ksi compression at this same location. Stresses due to spin (which is well below its maximum value at the time of peak setback) are negligible at this location. However, a combination of balloting and maximum spin (which occurs when setback acceleration is negligible) could produce a tensile hoop stress of 80 ksi about 2 in. from the aft end. The factors of safety for these combinations are 1.45 (balloting and setback) and 2.00 (balloting and spin) based on yield strength.

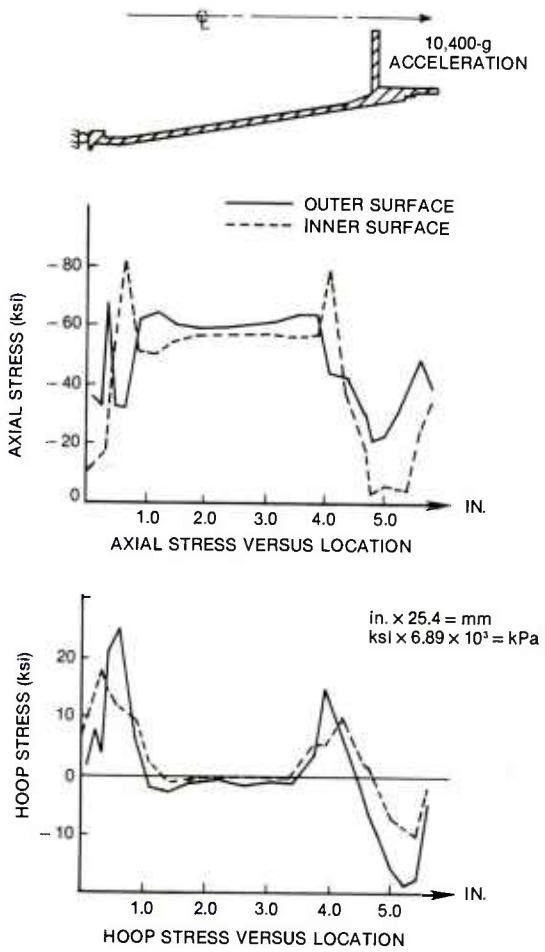

Figure 15. Stresses due to setback in center structure.

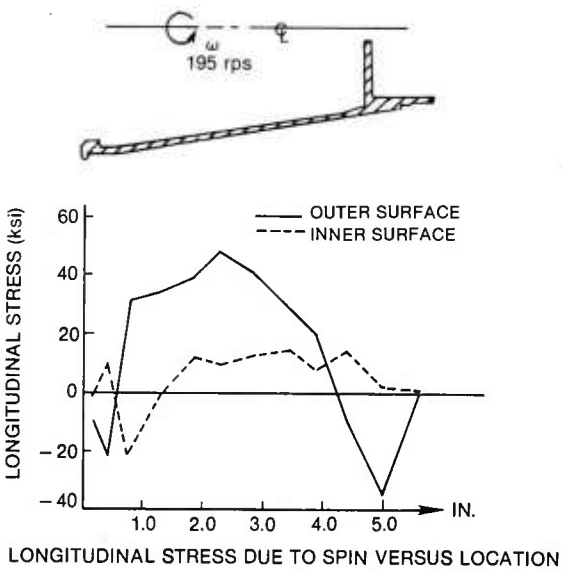

LONGITUDINAL STRESS DUE TO SPIN VERSUS LOCATION

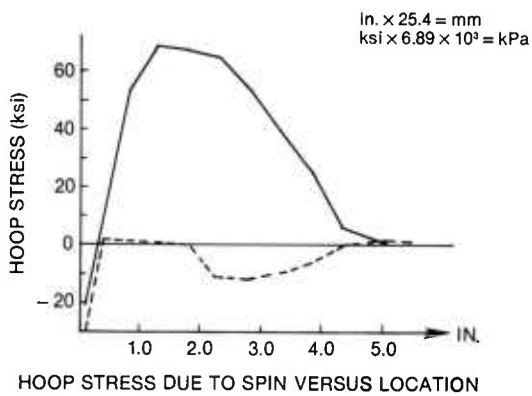

HOOP STRESS DUE TO SPIN VERSUS LOCATION

Figure 16. Stresses due to spin in center structure.

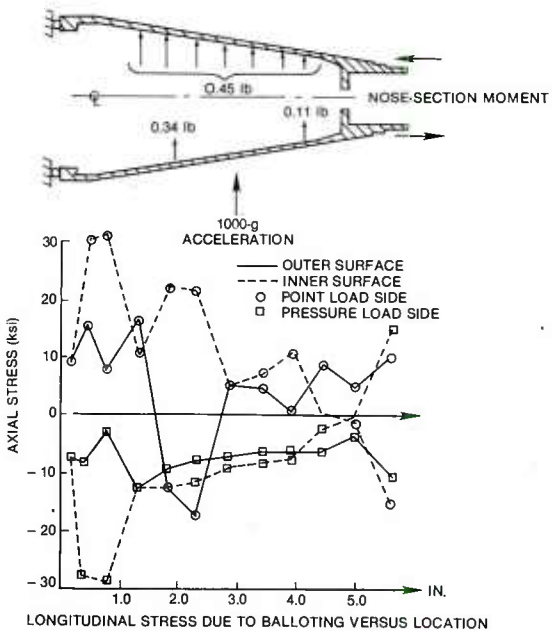

LONGITUDINAL STRESS DUE TO BALLOTING VERSUS LOCATION

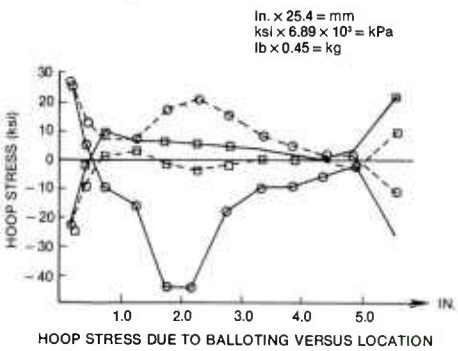

HOOP STRESS DUE TO BALLOTING VERSUS LOCATION

Figure 17. Stresses due to balloting in center structure.

5.3.2 *Target Sensor Assembly*

Each target sensor assembly consists of an rf chassis and sensor processor PWB. The rf chassis is seated on the center structure internal flange and is attached to its wall with two screws. A pin mounted in the center structure engages a slot in the rf housing to provide angular alignment and prevent rotation. The processor PWB is seated on the rf chassis lip and attached to the chassis with mounting screws at various locations on the board.

Stress levels and deflections in the processor PWB due to spin and balloting are negligible, since the board is well supported over its entire surface by the rf chassis. Setback-developed stresses at the base of the board are also relatively low (4 ksi) and well below the allowable stress for epoxy-fiberglass. Stress levels in the rf chassis are generally negligible. Setback-developed bearing stresses at the center structure support flange are 14 ksi, well below the allowable stress for 7075-T6 aluminum. Stresses in the support ledge for the processor PWB are also low (12.4-ksi bending and 4-ksi shear).

5.3.3 *Rear Collar Assembly*

The rear collar is a 6-6-2 titanium machined part which fastens the fuze to the projectile warhead section. The collar is captured between the center structure external flange or foot and the E1 assembly and cover, where a small gap allows free rotational movement. When assembled to the projectile warhead section, the rear collar clamps the center structure foot and rear structure to the projectile seating surface.

The rear collar was analyzed for balloting loads; stresses and deflections developed during other loading conditions are not significant and were not examined. The collar was modeled using plate elements, with only half of the part included due to symmetry. The maximum stress occurs near the aft end of the collar: 40-ksi compression in the axial direction. This is well below the allowable stress for 6-6-2 titanium.

5.4 *Rear Assembly*

The rear assembly consists of the programmer PWBs, the interconnection PWB, and the rear structure. The three vertically mounted programmer PWBs and the mating interconnection PWB are mounted to the rear structure. The programmer PWBs are fastened together by threaded studs with epoxy-fiberglass spacers at five locations throughout the PWBs and by two studs and four mounting blocks at the bottom corners. The assembly is attached to the rear structure with four screws, each fastened to a mounting block, from the bottom side of the structure. As in the M/T assembly, the blocks are located to insure that the programmer PWBs are seated firmly on the interconnection PWB. The programmer PWBs are constrained laterally by brackets mounted on the inside wall of the center structure, by the connector plates at the forward end of the center structure, and by two antiballoting screws which are secured against the center stud of the assembly from the target sensor assembly.

The rear structure is a 6-6-2 titanium machined part which supports the programmer PWBs, interconnection PWB, and the entire fuze center assembly and nose section. A closely controlled pilot diameter on the inside aft surface of the rear structure engages a similar diameter on the projectile, insuring concentric alignment and providing lateral support for the fuze. Four slots engage tabs in the projectile, providing angular alignment and preventing rotational motion during gun-launch angular acceleration.

The programmer PWBs were analyzed for setback, spin, and balloting loads. The rear structure analysis was confined to setback, since other loading conditions do not produce significant levels of stress or deflection in the structure. The setback analyses of the PWBs and the rear structure were performed in a series of iterative analyses. This was necessary to insure compatibility of boundary conditions (displacements and reaction forces) between the PWBs and the rear structure. Because of the relative compliance of the rear structure, the PWB reactions are confined to a small area near each corner, approximately 0.5 in. long. The reaction force varies approximately linearly from a peak at the corner to zero in a half-inch. Conversely, the board/structure deflections vary—from a peak

near the center of the rear structure to a much lower level at the board corner. However, the boards and structure are in contact over only the outer 0.5 in. during maximum setback loading.

Both the PWBs and the rear structure were analyzed with NASTRAN. The programmer PWBs were modeled with plate elements for balloting and spin, and membrane elements for setback. The finite-element model is depicted in figure 18.

Two different finite-element models were developed for the rear structure: ring element and plate element models. The use of ring elements permits the development of a very fine mesh model throughout the cross section of the part. This allows a detailed analysis of the stress distribution throughout the cross section. However, since these elements are limited to only two degrees of freedom (radial and axial), only uniform axisymmetrical loading and boundary conditions can be accommodated. Therefore, the ring element model was used only for the self-loading and center structure rim-loading conditions. The ring element model is shown in figure 19. The programmer PWB loading on the rear structure was analyzed using plate elements. Taking advantage of symmetry, a quarter-section of the structure was modeled as shown in figure 20. The results of these separate analyses were then superimposed to determine the resultant stress distribution in the rear structure.

As for the M/T PWBs, the stress levels in the programmer PWBs due to spin and balloting are low. In addition, the maximum out-of-plane deflections are well below the allowable 0.020 in. However, setback-developed stresses in the bottom corners are high (approximately 35 ksi). This is a very localized stress, which could result in a small amount of delamination of the multilayer PWB in this area. However, no significant crushing of the PWB material will occur once the stress levels redistribute as a result.

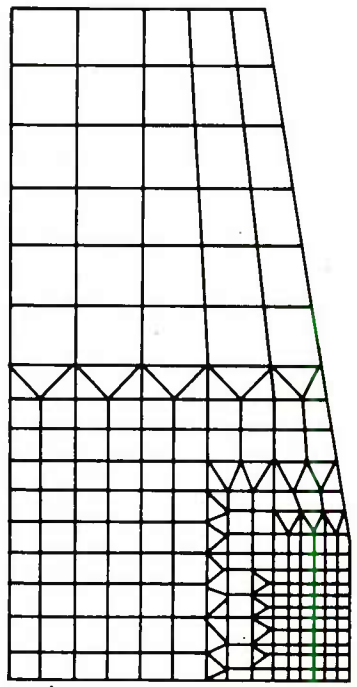

Figure 18. Programmer PWB model.

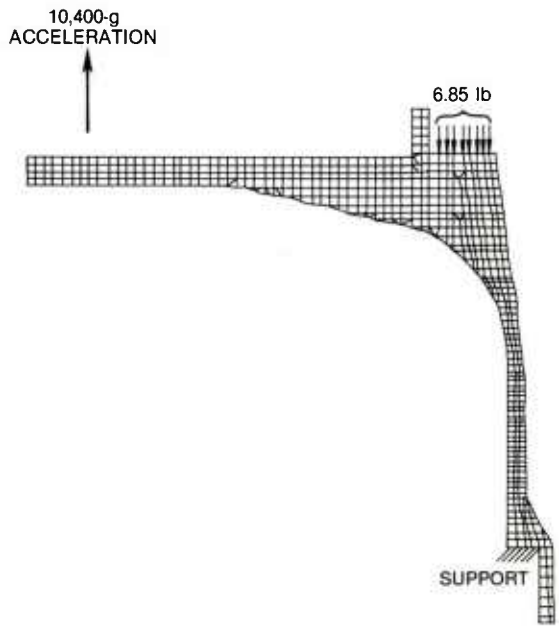

Figure 19. Rear structure finite element model with center assembly load during setback.

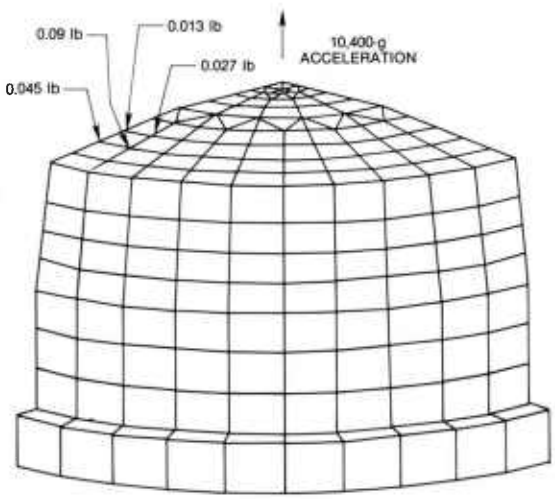

Figure 20. Rear structure model with programmer load during setback.

The combined analysis stress distribution for the rear structure is shown in figure 21. The maximum stress occurs in the outer wall near the aft end and is approximately 94 ksi, well below the allowable stress for titanium. Maximum deflections for the rear structure are plotted in figure 22. The maximum deflection at the center (0.043 in.) is well below the interface allowable (0.059 in.), and compares very well with the result obtained previously in the overall fuze analysis (0.044 in.).

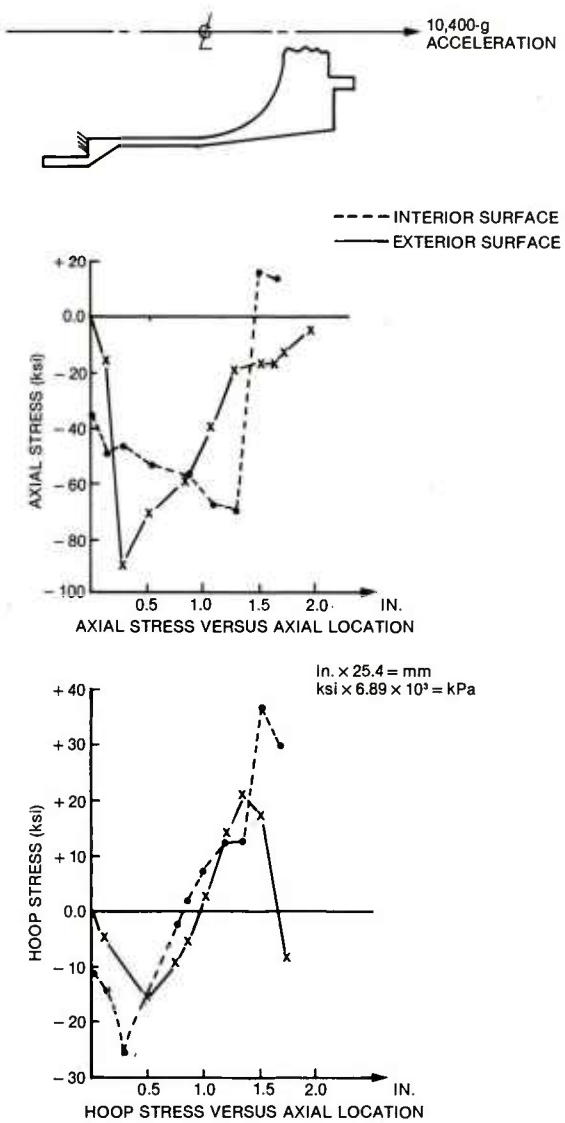

Figure 21. Combined stresses.

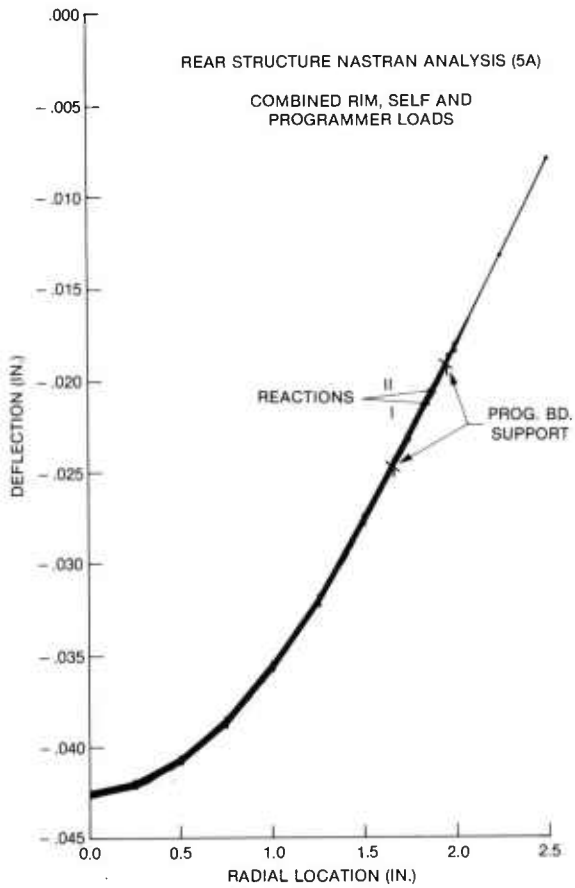

Figure 22. Rear structure NASTRAN analysis.

5.5 *Cover*

The fuze cover is a thin-walled epoxy-fiberglass shell. The cover is supported at its aft end for setback loading by a lip on the rear collar. An O-ring seated in the center structure thread relief retains the cover in place prior to installation of the fuze nose section. Pilot diameters at the front and aft ends align the cover concentrically with the fuze center structure. Since angular alignment is not critical, no keying is provided; the cover is free to rotate with respect to the fuze.

Setback and spin loading conditions were analyzed with an axisymmetric shell element model of the cover. Stresses and deflections developed as a result of other loading conditions are negligible. The maximum stress occurs near the base of the cover and is 7000 psi* compression in the meridional direction. The stress is the result of combined maximum setback with intermediate spin and is well below the material's allowable stress (15,000 psi).

5.6 *Miscellaneous*

There are a number of miscellaneous fasteners and pins used in the fuze for mounting and constraining subassemblies. The stresses for all of these were computed by conventional hand calculations. A summary of the resulting stresses is listed in table 1. A plastic limit analysis was performed for one fastener, the programmer PWB mounting stud. This analysis is described in appendix A.

6. LABORATORY TESTS

Laboratory stress tests were conducted for the power supply housing, center structure, and rear structure. These parts are the principal load-carrying structures, and were found to be the most highly stressed parts in the fuze. The purpose of the tests was to confirm the analytical predictions and verify the structural safety margin of the fuze design.

*(psi) 6.894 = (kPa).

TABLE 1. ASSEMBLY HARDWARE ANALYSIS SUMMARY

Part	Material	Load condition	Resulting stress (ksi[a])
Memory/timing (M/T) printed wiring board center stud	302 Stainless	Balloting	Compression, 30
M/T mounting block stud	17-4 PH stainless	Set forward	Shear, 10
M/T mounting block screws	M52463 carbon steel	Set forward	Tension, 15
Power supply housing flange pins	M516555 carbon steel	Angular acceleration	Bending, 13.4, shear, 17.7
Power supply housing base pins	303 stainless	Angular acceleration	Shear 37.3, bearing, 13.3
Connector plate screws	NA51352 alloy steel	Setback	Tension, 56.2
RF mounting screws	NA51352 alloy steel	Balloting	Tension, 103
RF pins	303 stainless	Angular acceleration	Shear, 30
Center structure pins	17-4 PH stainless	Angular acceleration	Bearing, 94.3, shear, 36
Programmer mounting block screws	NA51352 alloy steel	Set forward	Tension, 45
Programmer mounting block studs	Maraging steel	Set forward	Shear, 42, bending, 250[b]

[a] *(ksi) × 6.894 × 10^3 = (kPa).*
[b] *Designed with plastic limit analysis; see appendix A.*

The tests were performed with a hydraulic ram capable of producing loads up to 100,000 lb.* Applied force was measured by a digital-readout load cell placed under the test specimen support. Strains, and thereby stress levels, were measured with multiple strain gages attached at the appropriate locations of each part. A typical test setup is shown in figure 23.

(lb) 0.45 = (kg).

6.1 *Power Supply Housing*

The power supply housing was instrumented with strain gages at eight locations—three on the inside surface, two on the outer surface, and three on the connector shroud. Loads were applied to the bottom inside surface of the housing, simulating the setback loads of the two power supplies and the M/T assembly. In addition, loads were applied to the forward threads of the housing,

simulating the setback load of the forward structure. The housing was supported at the flange by a fixture which simulated the fuze center structure. Axial and hoop strains were recorded for each gage location, and figure 24 shows those for the housing sidewall plotted with the analytical predictions. Due to the extremely large stress gradients in these areas, only average stresses over the length of the gage could be recorded. As can be seen in the figure, the correlation between the analytical predictions and the experimental data is inconsistent. In general, the measured stress levels are significantly lower than the predictions.

6.2 *Center Structure*

The center structure was instrumented with strain gages at 10 locations—5 on the inner surface and 5 on the outer surface. Compressive load was applied to the forward surface of the structure to

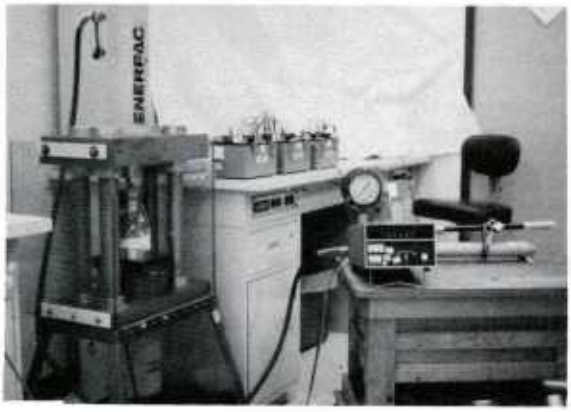

Figure 23. Typical test setup.

simulate the setback loading of the nose section. Additional loads were applied at that same location in increments to simulate the self-loading of the center structure at various axial locations. For example, strain readings were taken at the forward-most gages with a small additional load, whereas the aft gage readings were taken with an additional load equivalent to the entire center assembly.

The test results are plotted versus the analytical predictions in figure 25. In general, there is reasonable correlation between the experimental and analytical results. The most significant variance occurs near the aft end of the structure, where the measured axial stresses exceed the analytical predictions by 25 percent. This indicates higher bending stress levels in this area, probably due to a greater degree of fixity at the support for the center structure than was assumed for the boundary conditions in the finite-element analysis (simply supported). As a result, the actual factor of safety for the center structure may be slightly lower than predicted.

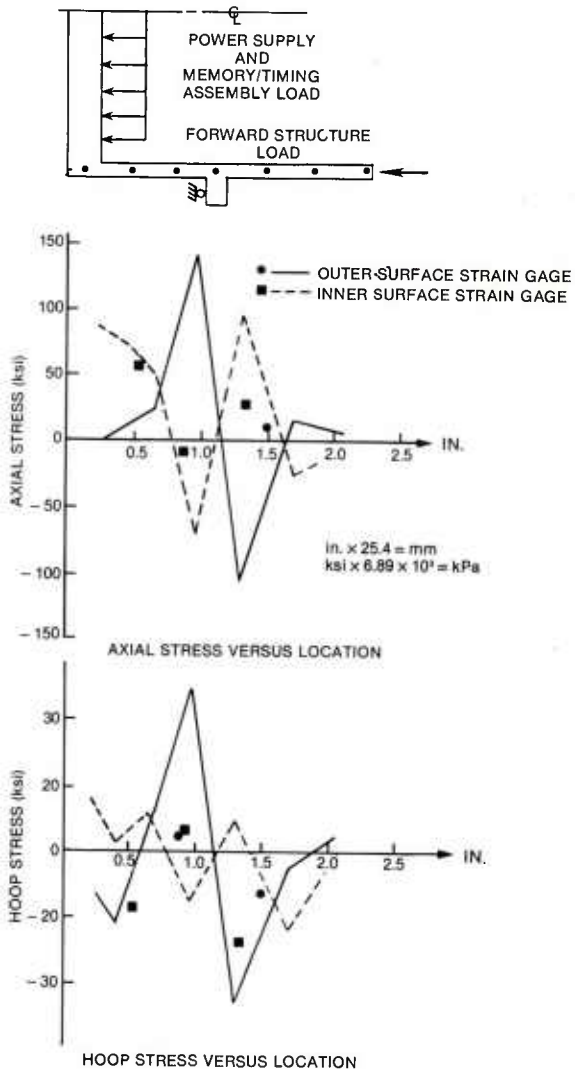

Figure 24. Static stress test results of power supply housing.

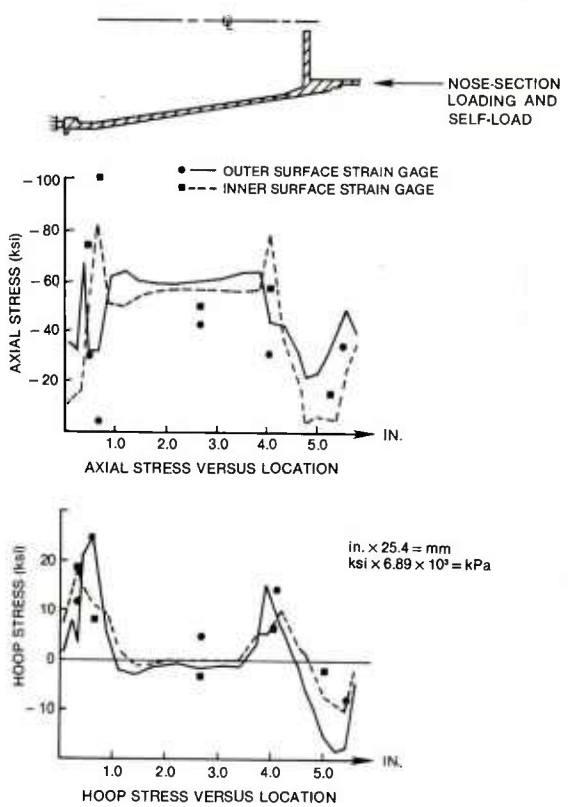

Figure 25. Static stress test results of center structure.

6.3 *Rear Structure*

The rear structure was instrumented with strain gages at 12 locations—6 on the inside surface and 6 on the outside surface. Compressive load was applied to the forward rim of the structure to simulate the setback loading due to the center structure.

The test results are plotted versus the analytical predictions in figure 26. In general, there is good agreement between the analytical results and the experimental data. The most significant difference between analytical and experimental data indicates higher (30 percent) bending stresses than predicted. As for the center structure, this is a localized high gradient condition which is probably due to a greater degree of fixity at the boundary than was assumed in the analysis (simply supported). A slight reduction in the calculated factor of safety appears likely.

7. SUMMARY AND CONCLUSIONS

The analysis results are summarized in table 2, which for each major part lists the material identification, yield and ultimate strengths, and respective safety factors. Each of the parts has a safety factor of 1.0 or greater; the most critical structural parts (the rear and center structures) exceed 1.5 for the ultimate safety factor. In general, those parts which exhibit safety factors only slightly larger than 1.0 do so only because of highly localized peak stresses. For example, the M/T and programmer PWBs are stressed highly in a very small area near their support point; these stresses diminish rapidly a short distance away. Several parts, such as the forward structure and collar, are very lowly stressed; these parts have been designed for minimum size and weight within the producibility constraints.

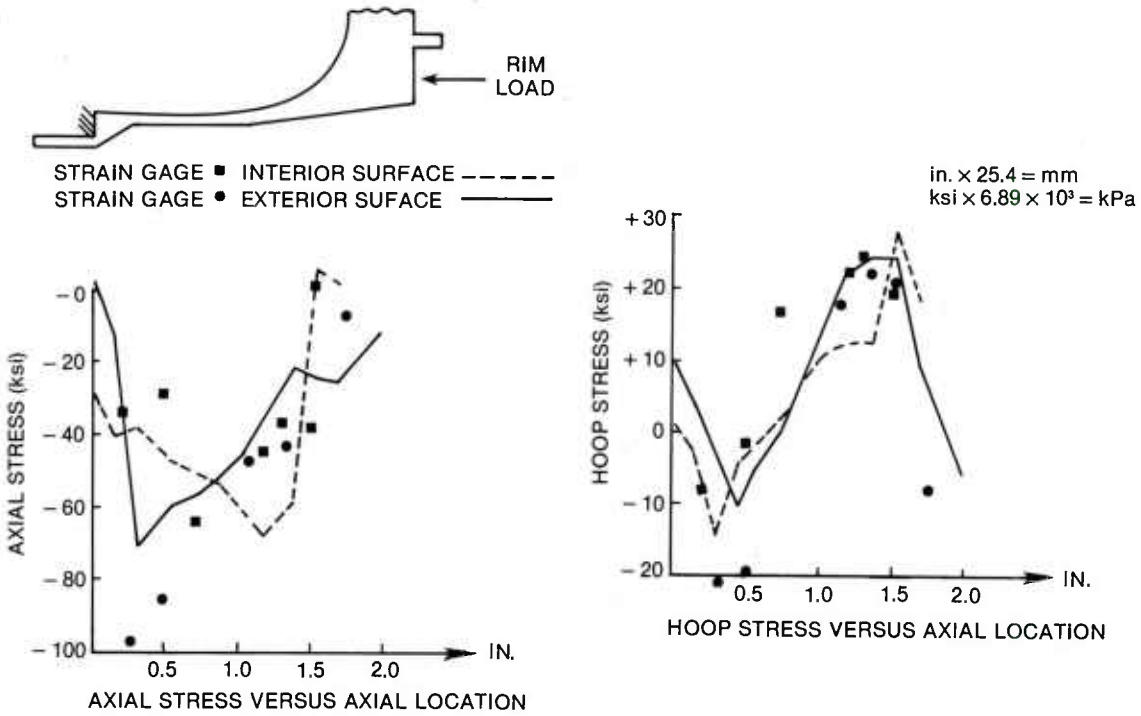

Figure 26. Static stress test results of rear structure.

The analytical predictions and safety factors were confirmed by the laboratory stress tests. Although there were some discrepancies in areas of large stress gradients, the overall correlation was acceptable.

In conclusion, the structural analysis and testing indicated that the M735 fuze design is structurally adequate and efficient. This conclusion has been subsequently verified by the successful gunfiring of over 250 fuzes without a single structural failure.

TABLE 2. SUMMARY OF ANALYSIS RESULTS

Component	Material	Strength[a]		Predicted minimum safety factor	
		Yield (ksi)	Ultimate (ksi)	Yield	Ultimate
Forward structure	6-6-2 titanium	160	175	(b)	(b)
Memory/timing printed wiring board	Epoxy-fiberglass	—	35	—	1.1
Memory/timing support plate	6-6-2 titanium	160	175	1.2	1.3
Power supply housing	6-6-2 titanium	160	175	1.15	1.25
Forward collar	6-6-2 titanium	160	175	(b)	(b)
Center structure	6-6-2 titanium	160	175	1.45	1.6
RF housing	7075-T6 aluminum	66	77	(b)	(b)
Sensor processor printed wiring board	Epoxy-fiberglass	—	35	(b)	(b)
Rear collar	6-6-2 titanium	160	175	4.0	4.4
Programmer printed wiring board	Epoxy-fiberglass	—	35	—	1.0
Rear structure	6-6-2 titanium	160	175	1.7	1.9
Cover	Epoxy-fiberglass	—	15	—	2.1

[a] *(ksi) 6.894 × 10^3 = (kPa).*
[b] *Part is not highly stressed; sized for manufacturing considerations.*

APPENDIX A.—PLASTIC LIMIT ANALYSIS OF THE PRINTED WIRING BOARD STUD

A plastic limit analysis was performed for the programmer printed wiring board (PWB) mounting stud. This analysis technique is used to determine the true load that a part can be expected to sustain without failure, while allowing some localized yielding.

The basic assumption used in limit analysis is that most engineering materials (e.g., steel, titanium, and aluminum) can be described as having elastic-perfectly plastic (E-PP) behavior. The material is assumed to behave elastically until it reaches its yield stress, and then stress remains constant regardless of the strain imposed. Although there is a limit to the amount of additional strain which can be imposed before failure, this is usually large compared to the strain at the yield point.

In a beam design governed by purely elastic analysis, the maximum allowable bending moment (M_e) is that which produces stress levels in the outer fibers at the yield point. At this level, however, stresses in the core of the beam are well below yield. If the moment is increased, the beam does not necessarily fail; rather, additional load is transferred to the inner fibers. In fact, additional loading can be tolerated until the total cross section yields. The bending moment which produces this condition is the limit or plastic moment (M_p).

For a circular cross-section beam (of radius r), the plastic moment is computed by multiplying the tensile yield strength by the plastic section modulus (Z), where Z is the sum of the area moments about the neutral axis. For an x-y coordinate system with its origin at the center of the cross section, Z can be computed as follows.

$$Z = \int_{-y}^{y} y \, dA \quad ,$$

where

$$dA = 2x \, dy = 2\sqrt{r^2 - y^2}\, dy \quad ,$$

$$Z = 4 \int_0^r y \sqrt{r^2 - y^2}\, dy \quad ,$$

$$Z = \frac{4r^3}{3} \quad .$$

The ratio of the plastic moment to the elastic moment is called the shape factor of the cross section and can be computed as follows.

$$\frac{M_p}{M_e} = \frac{\sigma_y Z}{\sigma_y I/c} = \frac{4r^3/3}{\pi r^4/4r} = \frac{16}{3\pi} \quad ,$$

$$\text{or } 1.698 \quad ,$$

where y is the material yield strength, I is the area moment of inertia, and c is the outer fiber distance from the neutral axis (r).

For the programmer PWB stud, the elastic moment is

$$M_e = \sigma_y I/c = \frac{(250{,}000)(7.7 \times 10^{-6})}{0.056} \quad ,$$

$$M_e = 34.4 \text{ in.-lb,}^*$$

and the plastic moment is therefore

$$M_p = 1.698 \, M_e = 58.4 \text{ in.-lb.}$$

The maximum moment applied to the stud was computed to be 48 in.-lb at the mounting block locations. Therefore, the stud safety factor is 1.2, based on this plastic limit analysis.

*(in.-lb) 0.113 = (N-m).

ADMINISTRATOR
DEFENSE TECHNICAL INFORMATION CENTER
ATTN DTIC-DDA (12 COPIES)
CAMERON STATION, BUILDING 5
ALEXANDRIA, VA 22314

US ARMY RSCH & STD (EUR)
ATTN CHIEF, PHYSICS & MATH BRANCH
FPO NEW YORK 09510

US ARMY ARMAMENT MATERIEL READINESS COMMAND
ATTN DRSAR-LEP-L, TECHNICAL LIBRARY
ATTN DRSAR-ASF, FUZE & MUNITIONS SUPPORT DIVISION
ROCK ISLAND, IL 61299

COMMANDER
US ARMY MISSILE & MUNITIONS CENTER & SCHOOL
ATTN ATSK-CTD-F
REDSTONE ARSENAL, AL 35809

DIRECTOR
US ARMY MATERIEL SYSTEMS ANALYSIS ACTIVITY
ATTN DRXSY-MP
ATTN DRXSY-RE, MR. G. J. GIBSON
ABERDEEN PROVING GROUND, MD 21005

DIRECTOR
US ARMY BALLISTIC RESEARCH LABORATORY
ATTN DRDAR-TSB-S (STINFO)
ATTN MR. R. LIESKE
ABERDEEN PROVING GROUND, MD 21005

US ARMY ELECTRONICS TECHNOLOGY & DEVICES LABORATORY
ATTN DELET-DD
FT MONMOUTH, NJ 07703

HQ USAF/SAMI
WASHINGTON, DC 20330

TELEDYNE BROWN ENGINEERING
CUMMINGS RESEARCH PARK
ATTN DR. MELVIN L. PRICE, MS-44
HUNTSVILLE, AL 35807

ENGINEERING SOCIETIES LIBRARY
ATTN ACQUISITIONS DEPARTMENT
345 EAST 47TH STREET
NEW YORK, NY 10017

COMMANDER
US ARMY MATERIEL DEVELOPMENT & READINESS COMMAND
ATTN DRCDE-DM, MR. C. RUBEN
5001 EISENHOWER AVENUE
ALEXANDRIA, VA 22333

HEADQUARTERS
DEPARTMENT OF THE ARMY
ATTN DAMA-CSS-N, LTC R. HARTER
WASHINGTON, DC 20310

COMMANDER
US ARMY NUCLEAR & CHEMICAL AGENCY
ATTN MONA-MS, LTC M. L. MOSBROOKER
7500 BACKLICK ROAD
BUILDING 2073
SPRINGFIELD, VA 22150

COMMANDER
US ARMY FIELD ARTILLERY BOARD
ATTN ATSF-CD-MW, MAJ J. RICCA
FT SILL, OK 73503

COMMANDER
US ARMY YUMA PROVING GROUND
ATTN STEYP-MTW, MR. M. MIRANDA
YUMA, AZ 85364

COMMANDER
US ARMY TEST & EVALUATION COMMAND
ATTN DRSTE-CM-F, MR. L. NEALLEY
ABERDEEN PROVING GROUND, MD 21005

COMMANDER
US ARMY ARMAMENT RESEARCH & DEVELOPMENT COMMAND
ATTN DRDAR-LCN-P, MR. C. SPINELLI
DOVER, NJ 07801

US ARMY ARMAMENT RESEARCH & DEVELOPMENT COMMAND
PROJECT MANAGER FOR NUCLEAR MUNITIONS
ATTN DRCPM-NUC, COL. FARMER
ATTN DRCPM-NUC, MR. K. WIDMAIER
DOVER, NJ 07801

SANDIA LABORATORIES
PO BOX 969
ATTN DIV 8167, MR. D. J. BOHRER
LIVERMORE, CA 94550

MOTOROLA, INC
GOVERNMENT ELECTRONICS DIVISION
PO BOX 1417
ATTN MR. A. KULVINSKAS
ATTN MR. J. McEOWN
ATTN MR. D. KIRK
SCOTTSDALE, AZ 85252

US ARMY ELECTRONICS RESEARCH &
DEVELOPMENT COMMAND
ATTN TECHNICAL DIRECTOR, DRDEL-CT

HARRY DIAMOND LABORATORIES
ATTN CO/TD/TSO/DIVISION DIRECTORS
ATTN RECORD COPY, 81200
ATTN HDL LIBRARY, 81100 (2 COPIES)
ATTN HDL LIBRARY, 81100 (WOODBRIDGE)
ATTN CHARIMAN, EDITORIAL COMMITTEE
ATTN TECHNICAL REPORTS BRANCH, 81300
(3 COPIES)
ATTN LEGAL OFFICE, 97000
ATTN CHIEF, 00210
ATTN LANHAM, C., 00213
ATTN WILLIS, B., 47400
ATTN DAVIS, H., 34600
ATTN PROBST, M., 36200
ATTN ANSTINE, C., JR., 15400
ATTN CRAWLEY, J., 36100
ATTN WESTLUND, R. E., 47000
ATTN OVERMAN, D. L., 34200
ATTN FRYDMAN, A. M., 48500
ATTN GOODMAN, R., 34400
ATTN INGERSOLL, P., 34300
ATTN TOKARCIK, J., 47500
ATTN NORTH, G., 47500
ATTN CRICKMAN, C., 36200
ATTN PEPERONE, S., 36000
ATTN DOCTOR, N., 34600
ATTN MILLER J., 36200 (5 COPIES)